View metadata, citation and similar papers at core.ac.uk
brought to you by CORE
provided by Florence Research

Near-Bed Turbulence Characteristics at the Entrainment Threshold of Sediment Beds

Subhasish Dey[1]; Sankar Sarkar[2]; and Luca Solari[3]

Abstract: This experimental study is devoted to quantification of the near-bed turbulence characteristics at an entrainment threshold of noncohesive sediments. Near the bed, the departure in the distributions of the observed time-averaged streamwise velocity from the logarithmic law is more for immobile beds than for entrainment-threshold beds. In the Reynolds shear stress distributions, a damping that occurs near the bed for sediment entrainment is higher than that for immobile beds. Quadrant analysis reveals that in the near-bed flow zone, ejections and sweeps on immobile beds cancel each other, giving rise to the outward interactions, whereas sweeps are the dominant mechanism toward sediment entrainment. The bursting duration for entrainment-threshold beds is smaller than that for immobile beds. On the other hand, the bursting frequency for entrainment-threshold beds is larger than that for immobile beds. The third-order correlations indicate that during sediment entrainment, a streamwise acceleration associated with a downward flux and advection of streamwise Reynolds normal stress is prevalent. The streamwise and the downward vertical fluxes of turbulent kinetic energy (TKE) increase with sediment entrainment. The TKE budget proves that for sediment entrainment, the pressure energy diffusion changes drastically to a negative magnitude, indicating a gain in turbulence production. **DOI: 10.1061/(ASCE)HY.1943-7900.0000396.** *© 2011 American Society of Civil Engineers.*

CE Database subject headings: Sediment transport; River beds; Turbulent flow; Fluvial hydraulics; Streamflow; Turbulence.

Author keywords: Fluvial hydraulics; River beds; Sediment transport; Stream beds; Stream flow; Turbulence; Turbulent flow.

Introduction

When a turbulent shear flow interacts with a sediment bed, the sediment particles on the bed surface are intermittently entrained at a random rate if the magnitude of the hydrodynamic forces acting on the sediment particles exceeds a certain threshold value. Since the pioneering work of Shields (1936), a number of studies have been carried out on entrainment threshold of sediment (White 1940; Fenton and Abbott 1977; Dey 1999; Dey et al. 1999; Zanke 2003). The entrainment threshold means the beginning of sediment motion by rolling or by short hopping. A state-of-the-art review on sediment threshold has been put forward by Dey and Papanicolaou (2008). In most of the previous studies, the flow velocity and the induced bed shear stress were characterized by the time-averaged form. Because of its simplicity, the time-averaged form allows the development of a straightforward entrainment-threshold criterion based on parameters that are relatively easy to determine. Nevertheless, the real hydrodynamic process causing sediment motion cannot be entirely characterized by this procedure. Recent studies reveal that the sediment motion associated with near-bed turbulence field induce a fluctuating nature of hydrodynamic forces that act on the sediment particles (Zanke 2003; Lu et al. 2005; Schmeeckle et al. 2007; Hofland and Battjes 2006; Dwivedi et al. 2010a, b; Detert et al. 2010).

The wall-shear layer of turbulent flows is characterized by a sequence of turbulent events known as *bursting phenomenon* (Kline et al. 1967; Robinson 1991). It represents a mechanism of turbulent energy generation near the wall (Nezu and Nakagawa 1993). Turbulent bursting phenomenon can be described as a sequence of quasi-cyclic process of ejection events, where the low-speed fluid streaks are ejected from the near-wall zone, and sweep events, where the high-speed fluid streaks move from upstream toward the wall, sweeping away the slowly moving fluid left from the preceding ejections. Thus, bursting phenomenon plays an important role on sediment entrainment. In fact, the discovery of the bursting phenomenon in turbulent flows created a new dimension in further studying the structures of wall turbulence and then applying the knowledge to explore the problem of sediment entrainment. In an attempt to link the characteristics of turbulent bursting with the entrainment threshold of sediments, some investigators suggested that the Reynolds shear stress component is not the most relevant mechanism to the sediment entrainment (Clifford et al. 1991; Nelson et al. 1995). Using hydrogen bubble visualization technique, Best (1992) attempted to link the sweeps with sediment entrainment and bed defect. The studies of Krogstad et al. (1992) and Papanicolaou et al. (2001) provided further evidence that the bed-packing conditions in gravel bed streams affect the turbulence characteristics and, in turn, sediment entrainment. Also, the quadrant analysis by Papanicolaou et al. (2001) showed that the ratio of the Reynolds shear stress to the streamwise turbulence intensity is smaller in the low-density packed beds than in the densely packed beds. Hence, the condition of the entrainment threshold based on the time-averaged bed shear stress criterion may give lower values, especially for the low-density packed beds. Recently, Dwivedi et al. (2010b) studied the entrainment of 39.7-mm-diameter spheres and observed the predominance of large sweeps at entrainment.

[1]Professor and Brahmaputra, Dept. of Civil Engineering, Indian Institute of Technology, Kharagpur 721302, West Bengal, India (corresponding author). E-mail: sdey@iitkgp.ac.in

[2]Doctoral Research Fellow, Dept. of Civil Engineering, Indian Institute of Technology, Kharagpur 721302, West Bengal, India. E-mail: sankar.iitkgp@gmail.com

[3]Assistant Professor, Dept. of Civil and Environmental Engineering, Univ. of Florence, via S. Marta 3, Firenze 50139, Italy. E-mail: luca.solari@dicea.unifi.it

Note. This manuscript was submitted on August 26, 2010; approved on January 28, 2011; published online on March 23, 2011. Discussion period open until February 1, 2012; separate discussions must be submitted for individual papers. This paper is part of the ***Journal of Hydraulic Engineering***, Vol. 137, No. 9, September 1, 2011. ©ASCE, ISSN 0733-9429/2011/9-945–958/$25.00.

Downloaded 13 Sep 2011 to 203.110.246.23. Redistribution subject to ASCE license or copyright. Visit http://www.ascelibrary.org

However, one of the key findings by Detert et al. (2010) that help understand the physical processes within a porous gravel bed (having a bimodal size distribution) toward the particle transport is the exponentially decaying nature of lift fluctuations with an increase in depth of the porous bed cover.

Despite the aforementioned recent attempts with large spheres or bimodal distribution of gravels, the role of turbulent coherent structures for the flow conditions corresponding to an entrainment threshold of riverine sediments seems to have received inadequate attention. Sutherland (1967) observed that sediment threshold is associated with a near-bed eddy impact onto the bed particles to produce a streamwise drag force that is large enough to roll the particles. The role of the turbulent structures on the bed-load transport was investigated by Heathershaw and Thorne (1985) in tidal channels. They argued that bed-load transport is not correlated with the instantaneous Reynolds shear stress but correlated with the near-wall instantaneous streamwise velocity. Field observations by Drake et al. (1988) on bed-load transport of gravels in alluvial streams suggested that majority of sediment transport is associated with sweep events that cause particle motion. These events occur very quickly at any location of the bed. Thus, sediment transport is episodic, with short periods of high transport and long periods of relatively feeble or no transport. Thorne et al. (1989) observed that the upward high-speed fluid streaks (known as *outward interactions*) play an important role on sediment entrainment. It is the instantaneous increase in streamwise velocity fluctuations that generate excess bed shear stresses, governing entrainment processes. Having studied the bed-load transport in nonuniform flows over two-dimensional dunes, Nelson et al. (1995) reported that the near-bed turbulence can change considerably, and hence the bed-load transport, whereas the bed shear stress remains almost unchanged. They observed that when the magnitude of the outward interactions increases relative to the sweep and ejection events, the sediment flux increases albeit the bed shear stress decreases. Cao (1997) proposed a model for sediment entrainment based on the characteristics of the bursting structures (with time and spatial scaling) that are inherent in wall turbulent flows. He argued that sediment entrainment is strongly dependent on shear velocity. Dey and Raikar (2007) studied the turbulence characteristics in flows over gravel beds near the threshold. They obtained the von Kármán constant as 0.35, which was different from its traditional value of 0.41 (also see Gaudio et al. 2010). Despite a number of serious efforts, there remain a lot of unanswered questions in quantifying the bursting events related to sediment entrainment and the role of near-bed turbulence on sediment threshold. In general, the basic problem of turbulent flows over a sediment bed starts in a deceptively simple way: Given the sediment size, flow rate, and bed slope, what is the probable amount of sediment transported? Even for the simplest case of a two-dimensional bed formed by uniform sediments, a general solution can only be presented, with estimates involving a high degree of uncertainty, as much of the intricacy lies on the consideration of the contributions from the conditional Reynolds shear stresses near the sediment beds. Thus, the primary motivation of this study lies on an appropriate quantification of the near-bed bursting phenomenon, so that future researchers can develop an improved theory that can produce a reasonable estimate for sediment transport.

This study addresses how the turbulence characteristics in near-bed flows respond to an entrainment threshold of noncohesive sediments, providing important results pertaining to bursting events. The flux and advection of normal stresses, turbulent kinetic energy flux, and energy budget, which are also key parameters for understanding the turbulence processes, are also studied to examine the bursting events comprehensively. Analysis of experimental data, measured by a Vectrino probe in flows over immobile and entrainment-threshold sediment beds, reveals the changes in the turbulence characteristics caused by the difference in bed conditions. The experimental data for flows over immobile beds are used as reference.

Experimental Setup and Procedure

Experiments were carried out in a rectangular open-channel flume with glass walls [Fig. 1(a)]. The flume was 0.6 m wide, 0.71 m deep, and 12 m long. An electromechanically operated sediment feeder that had a hopper and a conveyer belt as main components was installed near the inlet of the flume to feed sediments into the flow. A speed regulator for the roller that drove the conveyer belt regulated the uniform sediment–feeding rate. The sediments transported by the flows were collected in a downstream sediment collector. The 0.1-m-thick bed was created by using uniform sediments. Individual sediment samples used in the experiments had median diameters of $d_{50} = 1.97$, 2.92, 4.1, and 5.53 mm. The degree of uniformity of the particle-size distribution of a sediment sample is defined by the value of the geometric standard deviation σ_g estimated by $(d_{84}/d_{16})^{0.5}$, which is less than 1.4 for a uniform sediment (Dey et al. 1995) (see Table 1). Three different streamwise bed slopes ($S = 0.083$, 0.143, and 0.286%) were used. The incoming flow rate was controlled by an inlet valve and measured by a calibrated V-notch weir. A desirable normal flow depth over the bed was obtained by controlling the flow depth by an adjustable tailgate located at the downstream end of the flume. The experimental setup was designed to ensure a uniform flow over the sediment beds; a test section was considered by measuring flow depths within the reach of 6–9 m from the flume entrance. For each sediment sample, an experimental set comprised two different experimental runs for immobile and entrainment-threshold bed conditions. For tests with entrainment-threshold beds, the threshold condition was ensured when the surface particles had feeble movement over a period of time. According to the U.S. Army Engineers Waterways Experiment Station (USWES 1936), entrainment threshold, defined as the sediments in motion, should reasonably be represented by all sizes of bed particles and that the sediment flux should exceed 4.1×10^{-4} kg/(m · s). Therefore, in this study, a certain degree of established weak transport (slightly greater than 4.1×10^{-4} kg/(m · s)) of bed particles was considered as an entrainment-threshold condition. The mode of sediment movement was mainly observed as rolling and hopping motion of particles in contact with the bed. Once the inflow rate corresponding to the desirable bed condition (immobile or entrainment threshold) was set, the velocity measurements were undertaken. For an entrainment-threshold condition, the sediment-transport rate was initially quantified from the bed particles collected in the downstream collector for 5 min. Once the sediment was collected, it was dried and weighed to determine the transport rate. The sediment feeding was operated at the same rate as the sediment transport. During the experiments, no changes in the bed elevation corresponding to an entrainment-threshold condition were obvious, as the feeding or transport of sediment was too small. In this way, during the tests, the beds remained in dynamic equilibrium under an entrainment-threshold condition. The flow depth h is the vertical distance from the virtual bed level to the free surface. The virtual bed level, which is the reference of the vertical distance ($z = 0$), was considered at $0.25d_{50}$ below the top level of the bed particles. Van Rijn (1984) reported that a log law over a sediment bed could be preserved by fixing a virtual bed level at $0.25d_{50}$ below the top level of the bed particles.

Downloaded 13 Sep 2011 to 203.110.246.23. Redistribution subject to ASCE license or copyright. Visit http://www.ascelibrary.org

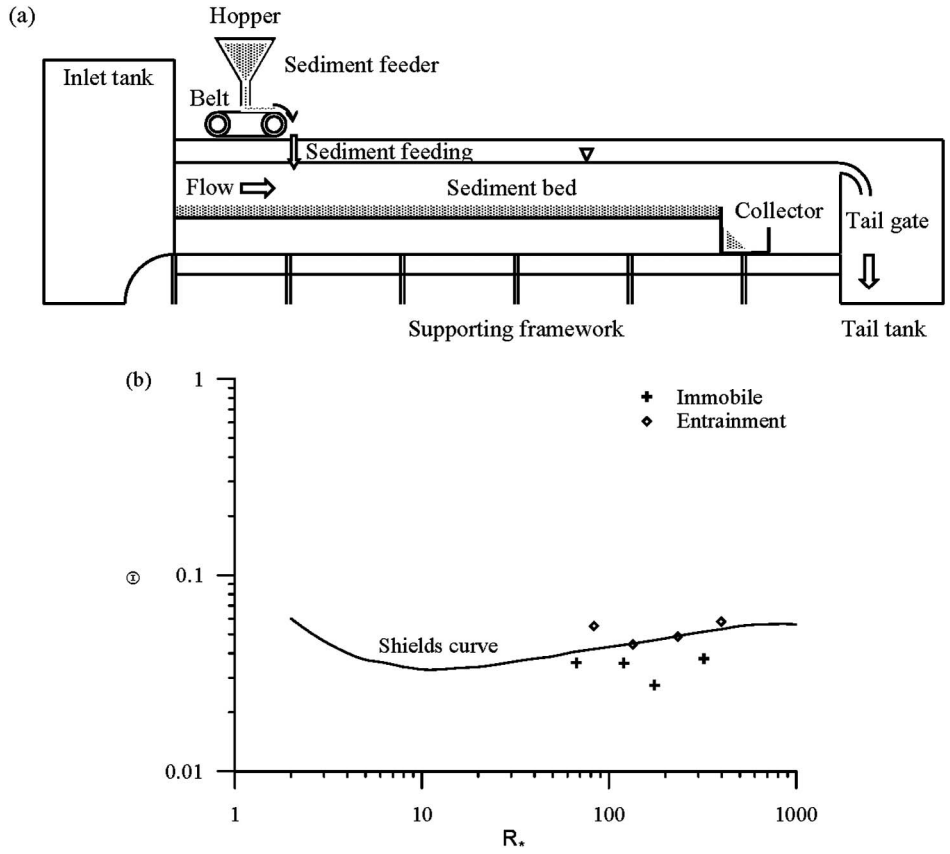

Fig. 1. (a) Schematic of experimental setup; (b) experimental data plots on Shields diagram

Table 1. Characteristics of Sediments Used in Experiments

d_{50} (mm)	d_{16} (mm)	d_{84} (mm)	Relative density	σ_g	Angle of repose (degree)	u_{*c} (ms^{-1})[a]
1.97	1.65	2.7	2.65	1.28	29	0.036
2.92	2.48	3.63	2.65	1.2	30	0.046
4.1	3.55	4.52	2.65	1.13	32.5	0.058
5.53	4.91	6.09	2.65	1.1	34	0.07

[a]u_{*c} = critical shear velocity obtained from the Shields diagram.

The ranges of relative submergence $S_h = d_{50}/h$, flow Reynolds number $\mathsf{R} = 4hU/\upsilon$ (where U = depth-averaged velocity; and υ = kinematic viscosity of fluid), flow Froude number $\mathsf{F} = U/(gh)^{0.5}$ (where g = gravitational acceleration), and densimetric Froude number $\mathsf{F}_d = U/(\Delta g d_{50})^{0.5}$ (where Δ = submerged relative density of sediment) were studied for $0.009 \le S_h \le 0.046$, $2.744 \times 10^5 \le \mathsf{R} \le 7.084 \times 10^5$, $0.42 \le \mathsf{F} \le 0.61$, and $2.21 \le \mathsf{F}_d \le 3.42$, respectively. The shear-particle Reynolds numbers $\mathsf{R}_* = d_{50}u_*/\upsilon$ (where u_* = shear velocity) were generally greater than 70, implying that the flow conditions were turbulent-rough. Table 2 gives the important experimental parameters of different sets. In an entrainment-threshold bed, the shear velocities $u_{*1} = (ghS)^{0.5}$ determined from the bed slope nearly correspond to the critical shear velocities obtained from the Shields diagram,

Table 2. Experimental Data

Set	Bed condition	d_{50} (mm)	S (%)	h (m)	U (ms^{-1})	u_{*1} (ms^{-1})	u_{*2} (ms^{-1})	λ	R	R_*	F	F_d	S_h	q_s (kgm^{-1}s^{-1})
1	Immobile	1.97	0.083	0.14	0.49	0.0338	0.034	0.039	2.744×10^5	67	0.42	2.74	0.014	—
	Entrainment	1.97	0.083	0.215	0.61	0.0419	0.0296	0.019	5.246×10^5	83	0.42	3.42	0.009	0.00144
2	Immobile	2.92	0.143	0.12	0.54	0.041	0.0412	0.047	2.592×10^5	120	0.5	2.48	0.024	—
	Entrainment	2.92	0.143	0.15	0.63	0.0458	0.036	0.026	3.78×10^5	134	0.52	2.9	0.019	0.00183
3	Immobile	4.1	0.143	0.13	0.6	0.0427	0.0429	0.041	3.12×10^5	175	0.53	2.33	0.032	—
	Entrainment	4.1	0.143	0.23	0.77	0.0568	0.0424	0.024	7.084×10^5	233	0.51	2.99	0.018	0.00165
4	Immobile	5.53	0.286	0.12	0.66	0.058	0.058	0.062	3.168×10^5	321	0.61	2.21	0.046	—
	Entrainment	5.53	0.286	0.185	0.81	0.072	0.046	0.026	5.994×10^5	398	0.6	2.71	0.03	0.00245

Note: For entrainment-threshold bed condition, the values of sediment transport rate q_s are nonzero. u_{*1} and u_{*2} = shear velocities obtained from the bed slope and Reynolds shear stress profiles, respectively; and λ = bed friction factor.

Downloaded 13 Sep 2011 to 203.110.246.23. Redistribution subject to ASCE license or copyright. Visit http://www.ascelibrary.org

Table 3. Uncertainty Estimation for Vectrino

d_{50}(mm)	Bed condition	u (cms^{-1})	v (cms^{-1})	w (cms^{-1})	$(\overline{u'u'})^{0.5}$(cms^{-1})	$(\overline{v'v'})^{0.5}$ (cms^{-1})	$(\overline{w'w'})^{0.5}$ (cms^{-1})	$\overline{u'w'}$ (cm^{2}s^{-2})
1.97	Immobile	0.35[a]	0.252	0.173	0.176	0.129	0.077	0.678
		(±2.76)[b]	(±3.13)	(±3.28)	(±2.39)	(±3.57)	(±1.83)	(±5.39)
	Entrainment	0.343	0.227	0.195	0.217	0.138	0.068	0.783
		(±3.32)	(±3.96)	(±3.78)	(±2.33)	(±4.03)	(±1.76)	(±5.31)
5.53	Immobile	0.325	0.243	0.126	0.173	0.118	0.063	0.698
		(±2.08)	(±2.98)	(±3.21)	(±2.12)	(±3.57)	(±1.65)	(±5.13)
	Entrainment	0.309	0.218	0.156	0.104	0.131	0.058	0.659
		(±2.16)	(±2.39)	(±3.21)	(±2.01)	(±3.42)	(±1.57)	(±4.99)

[a]Standard deviation.
[b]Average of maximum (negative and positive) percentage error.

whereas the shear velocities $u_{*2} = (-\overline{u'w'})^{0.5}|_{z=0.25d_{50}}$ (where u' and w' = fluctuations of instantaneous streamwise and vertical velocity components, respectively) obtained from the Reynolds shear stress measurements are generally less than those obtained from the bed slope. Henceforth, the notation u_{*2} is replaced by u_*. The reason for the discrepancy in shear velocities is discussed in the following section. Fig. 1(b) shows the data plots of Shields parameter Θ versus R_* overlapped on the Shields diagram. It is obvious that the data plots for the entrainment-threshold beds lie on or above the Shields curve, whereas those for immobile beds belong below the Shields curve.

A four-beam Vectrino probe (down-looking acoustic Doppler velocimeter; Nortek, Annapolis, MD) was used to capture the instantaneous velocity components. It worked with an acoustic frequency of 10 MHz. The data were measured at a sampling rate of 100 Hz. The sampling volume was cylindrical, having 6 mm diameter and 1–4 mm adjustable height. The sampling rate could be magnified up to 200 Hz, but it was experienced that the sampling rate of 100 Hz produced least noise in the signals. As the measuring location was 5 cm below the probe, the influence of the probe on the measured data was minimal. The data samplings were made over a duration of 300 s to achieve a statistically time-independent averaged quantities. In the near-bed flow zone, the sampling length used was 1 mm. The closest measuring location to the bed was always $z = 3$ mm, which ensured that the sampling volume did not touch the sediment particles while the points of measurements were quite close to the bed. In the upper flow zone $\hat{z} > 0.2$ (where $\hat{z} = z/h$), the sampling length used was 4 mm. The measurement within the top 5-cm flow layer was not possible because of the limitation of the Vectrino probe. The measurements were taken along the vertical line at the mid–cross section of the flume at a distance of 7.5 m from the entrance. Such an arrangement helped avoid transverse gradients of velocity, satisfying the two-dimensional flow criterion. To check the two-dimensionality of the flow, some velocity measurements were also taken at different transverse distances for certain streamwise locations. An examination of the velocity distributions revealed that in the middle portion of the flume (up to ±0.2 m on either side of the plane of symmetry of the flume), the flow was plausibly two-dimensional. The uncertainty of the Vectrino data (Table 3) was estimated by testing 10 samples collected at a sampling rate of 100 Hz for 300 s. These samplings were made at a location of $z = 5$ mm over the beds of sediment sizes $d_{50} = 1.97$ and 5.53 mm. In Table 3, v' = fluctuation of instantaneous lateral velocity component; $(\overline{u'u'})^{0.5}$ = RMS of u'; $(\overline{v'v'})^{0.5}$ = RMS of v'; $(\overline{w'w'})^{0.5}$ = RMS of w'; and $-\overline{u'w'}$ = Reynolds shear stress (divided by the mass density ρ of fluid). To avoid bias and random errors of the experimental setup, measurements were taken at different times after resuming the experiments. The data shown in Table 3 corroborate the capability of a 100-Hz sampling frequency for Vectrino measurements.

In the near-bed flow zone, the data measured by the Vectrino probe sometimes contained spikes because of the interference between incident and reflected pulses. Therefore, the data were filtered by a spike-removal algorithm. Throughout the experiments, the signal-to-noise ratio was maintained at 17 or above. In general, the signal correlations between transmitted and received pair of pulses were greater than 70%, which was the recommended cutoff value. However, near the bed, the range of the signal correlations was $70 \pm 5\%$ because of the occurrence of possible steep velocity gradient within the sampling volume. By using the discrete fast Fourier transforms, velocity power spectra $S_{ii}(f)$ [e.g., $S_{uu}(f)$ for u] were calculated. Fig. 2 presents $S_{ii}(f)$ at the nearest point to the bed ($z = 3$ mm) and at the top of the wall-shear layer ($\hat{z} = 0.2$) in the flows over immobile and entrainment-threshold beds for Set 3. The power spectra of these signals exhibited a more or less satisfactory fit with Kolmogorov "$-5/3$" scaling law in the inertial subrange of frequency that exists for frequencies $f > 10$ Hz. An interesting feature is that the turbulent events apparently contribute a "-1" scaling law where the energy production and cascade energy transfer coexist (Nikora 1999). These features confirm the adequacy of the Vectrino measurements within the near-bed flow zone. At low frequencies, the power spectra exhibit similar relationships between velocity components, where $S_{uu}(f) > S_{vv}(f) > S_{ww}(f)$. No discrete spectral peak was apparent at frequencies greater than 0.5 Hz (only a spectral band is obtained). It suggests that the signals less than 0.5 Hz were associated with large-scale motions, whereas those greater than 0.5 Hz were associated with pure turbulence. In this study, the measured raw data were therefore processed by using a high-pass filter with a cutoff frequency of 0.5 Hz, a correlation threshold, and a spike-removal algorithm. Importantly, there is no obvious difference in $S_{ii}(f)$ in the flows over immobile and entrainment-threshold beds. Thus, the velocity power spectra were not contaminated by the entrained sediments toward a threshold condition. For the ratio of flume width to flow depth of less than 6, the wall-affected zones (wedge shaped) from the two side walls of the flume start encroaching near the free surface, developing a dip in velocity profile (Yang et al. 2004). As the focus of this study, where flume width/flow depth ≈3–5 was on the near-bed flow zone (mainly wall-shear layer), the wall-affected zone remained in the top portion of the flow.

Time-Averaged Velocity and Reynolds Shear Stress

Figs. 3(a) and 3(b) show the vertical distributions of normalized time-averaged streamwise velocity and Reynolds shear stress in flows over immobile and entrainment-threshold beds. Despite a

Downloaded 13 Sep 2011 to 203.110.246.23. Redistribution subject to ASCE license or copyright. Visit http://www.ascelibrary.org

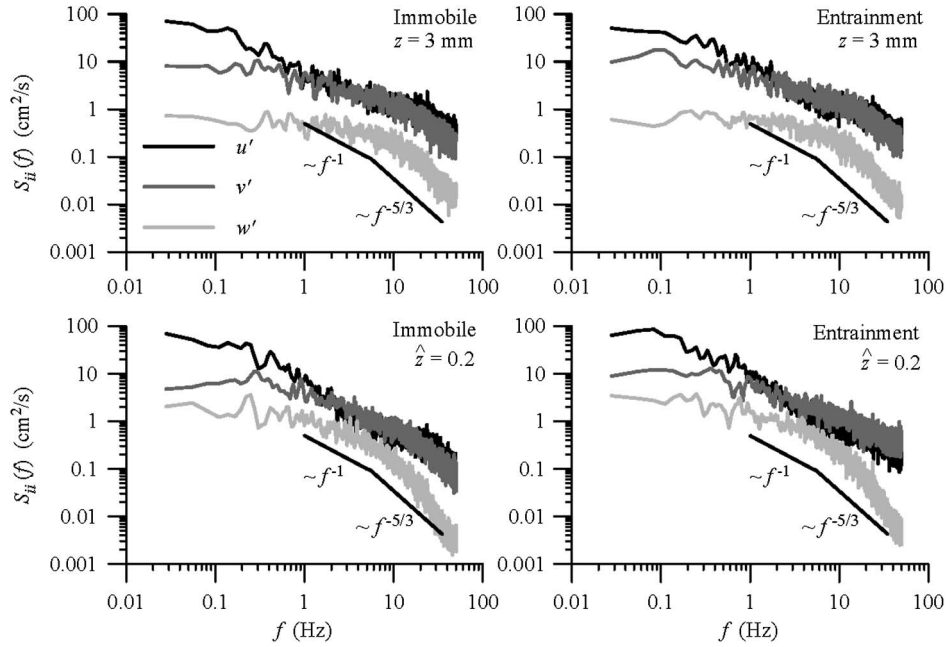

Fig. 2. Velocity power spectra $S_{ii}(f)$ for Set 3

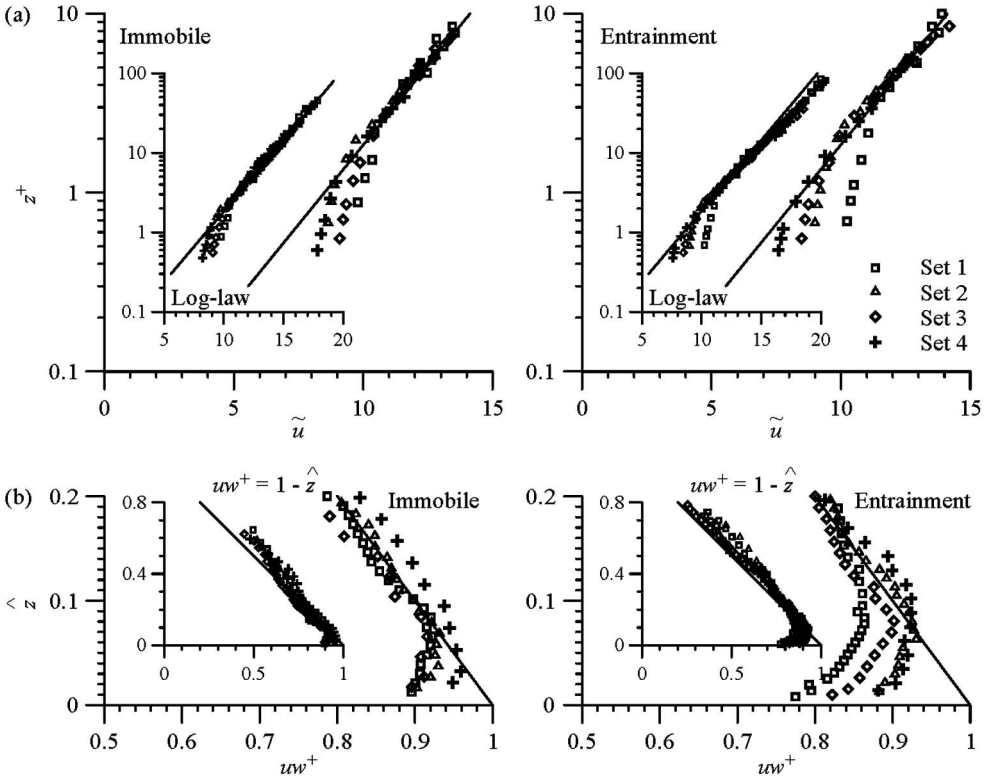

Fig. 3. Vertical distributions of (a) normalized time-averaged streamwise velocity $\tilde{u}$ and (b) normalized Reynolds shear stress uw^+

number of studies on flows over immobile and mobile beds (Song et al. 1994; Nikora and Goring 2000; Dey and Raikar 2007), they were not specifically focused on the near-bed turbulent flow characteristics. The shear velocities u_*, determined from the measured Reynolds shear stress distributions extrapolating them to the bed, are used to scale the velocity and the Reynolds shear stress (Table 2). As the primary focus of this study is on the turbulence characteristics, the shear velocities determined from the Reynolds shear stress distributions are preferred to those obtained from the bed slopes. Importantly, Reynolds shear stress distributions give a clear idea on the truly available shear stress in the flowing fluid. Fig. 3(a) describes the variations of normalized time-averaged streamwise velocity $\tilde{u} = u/u_*$ (where u = time-averaged streamwise velocity) with normalized vertical distance $z^+ = z/d_{50}$. As the flow regime tested was the turbulent-rough flow, d_{50} is used to scale the vertical distance. To have a clear view of the

Downloaded 13 Sep 2011 to 203.110.246.23. Redistribution subject to ASCE license or copyright. Visit http://www.ascelibrary.org

near-bed velocity distributions, the data plots are shown up to $z^+ = 10$ in a larger scale, although an extended view of all the data plots is also depicted in the insets. Within the wall-shear layer, the data plots for $z^+ > 3$ collapse on the logarithmic law $[\tilde{u} = 2.43\ln(z^+) + 8.5]$ of the rough wall, whereas those for $z^+ \leq 3$ are underestimated by the logarithmic law. The departure of data plots from the logarithmic law is attributed to the flow roughness layer that exists near the bed with a thickness of 2–5d_{50} (Raupach et al. 1991; Nikora et al. 2001). It is evident that in this layer, the departure of data plots from the logarithmic law for immobile beds is higher than that for entrainment-threshold beds. This is concluded on the basis of the majority of the data trends for different sets, although the data plots for Set 1 exhibit a slightly different feature. In Fig. 3(b), the distributions of normalized Reynolds shear stress $uw^+(= -\overline{u'w'}/u_*^2)$ are also shown for the wall-shear layer ($\hat{z} < 0.2$) in a larger scale. Here, flow depth h is used to scale the vertical distance z, as is considered in the linear law of $-\overline{u'w'}$ (that is, $uw^+ = 1–\hat{z}$) for free-surface flows with a zero-pressure gradient. Near the bed, the distributions of uw^+ for immobile and entrainment-threshold beds have a strong departure from the linear law of $-\overline{u'w'}$. On the other hand, in the upper flow zone, the plotted data are reasonably consistent with the linear law, although they have a slight tendency to exceed the law. For $\hat{z} < 0.1$ (near the bed), $-\overline{u'w'}$ for entrainment-threshold beds diminishes more than for immobile beds. In Table 2, the values of shear velocity u_* obtained from the bed slopes and those obtained from $-\overline{u'w'}$ distributions for immobile beds are fairly comparable. On the other hand, for entrainment-threshold beds, the shear velocities u_* obtained from $-\overline{u'w'}$ distributions are consistently less than those obtained from the bed slope or the critical shear velocities u_{*c} determined from the Shields diagram, but the values of u_* determined from the bed slopes correspond to those of u_{*c}. The reduction in the magnitude of u_* for entrainment-threshold beds is attributed to a portion of the fluid turbulent stress transferred to the bed particles to overcome the frictional resistance at the contacts of the entrained sediment particles. This is analogous to the concept of Grass (1970). The damping of the bed shear stress in terms of the Reynolds shear stress can also be explained by the fact that the bed particles are associated with the provided momentum for the flow to maintain their motion (Yeganeh-Bakhtiary et al. 2000, 2009). This concept can be examined through a simple mathematical exercise for the weak entrainment of sediment particles from the data given in Table 2. If the bed is immobile, the total bed shear stress τ obtained from the bed slopes is balanced by the sum of the bed shear stress of fluid τ_f and that of particles τ_s to overcome frictional resistance. Therefore, one gets $\tau_s = \tau - \tau_f$ with $\tau_s = \mu(1-s)\rho g(\pi d_{50}^3/6)\xi n$ and $\tau - \tau_f = \rho(u_{*1}^2 - u_{*2}^2)$, where μ = Coulomb friction factor; s = relative density of sediments; ξ = fraction of particles entrained per unit area; n = number of bed particles per unit area, that is, $(1-\rho_0)/(\pi d_{50}^2/4)$; and ρ_0 = porosity of sediments. The values of ξ calculated for Sets 1, 2, 3, and 4 are 0.12, 0.074, 0.093, and 0.127, respectively, which give rise to the measured transport rate q_s given in Table 2. Additionally, the estimated values of friction factor $\lambda(= 8u_*^2/U^2)$ are listed in Table 2, where λ decreases when there is sediment entrainment. From the viewpoint of the physics of flow, it is intuitive that because of slip or motion of the bed particles, the resistance to the flowing fluid from a mobile bed is always less than that from an immobile bed. Thus, the contradictory findings of Song et al. (1994, 1998), who argued that the friction factor increases with sediment transport may invite uncertainty. They calculated u_* from the bed slopes, suggesting that the calculation of u_* from the bed slopes is valid only for immobile beds and cannot truly predict u_* for mobile beds because the original derivation of $u_* = (ghS)^{0.5}$ is based on a rigid wall (Streeter and Wylie 1983).

Quadrant Analysis for Conditional Reynolds Shear Stresses

The bursting events are determined from the conditional statistics of the velocity fluctuations u' and w'. It is thus necessary to plot the data of u' corresponding to w' according to quadrants on $u'w'$-plane (Lu and Willmarth 1973) [Fig. 4(a)]. To discriminate the larger contributions to $-\overline{u'w'}$ from each quadrant discarding the smaller u' and w' corresponding to more quiescent periods, a hole-size parameter H is used (Nezu and Nakagawa 1993). The hyperbolic hole region is determined by the curve $|u'w'| = H(\overline{u'u'})^{0.5}(\overline{w'w'})^{0.5}$ [Fig. 4(a)]. Thus, a clear distinction is possible between the strong and the weak events for a small hole size and only strong events for a large hole size. The four quadrants i = 1, 2, 3, and 4 characterize the types of bursting event: (1) outward interactions Q1 ($i = 1$; $u' > 0, w' > 0$); (2) ejections Q2 ($i = 2$; $u' < 0, w' > 0$); (3) inward interactions Q3 ($i = 3$; $u' < 0, w' < 0$); and (4) sweeps Q4 ($i = 4$; $u' > 0, w' < 0$). The hole size $H = 0$ means that all data pairs (u', w') are taken into consideration. The quadrant analysis therefore provides an estimation of the fractional contributions to $-\overline{u'w'}$ from the bursting events.

Involving a detection function $\lambda_{i,H}(z,t)$ given by

$$\lambda_{i,H}(z,t) = \begin{cases} 1, & \text{if } (u',w') \text{ is in quadrant } i \text{ and if } |u'w'| \geq H(\overline{u'u'})^{0.5}(\overline{w'w'})^{0.5} \\ 0, & \text{otherwise} \end{cases} \quad (1)$$

the contributions to $-\overline{u'w'}$ from the quadrant i outside the hole region of size H is estimated by

$$\langle u'w' \rangle_{i,H} = \lim_{T\to\infty} \frac{1}{T} \int_0^T u'(t)w'(t)\lambda_{i,H}(z,t)dt \quad (2)$$

where T = sampling duration. Thus, the fractional contribution $S_{i,H}$ to $-\overline{u'w'}$ from each event is

$$S_{i,H} = \langle u'w' \rangle_{i,H} / \overline{u'w'} \quad (3)$$

Here, if $S_{i,H} > 0$, then $i = 2$ and 4 (Q2 and Q4); and if $S_{i,H} < 0$, then $i = 1$ and 3 (Q1 and Q3).

Fig. 4(b) shows the vertical distributions of fractional contribution $S_{i,0}$ of the Reynolds shear stress in flows over immobile and entrainment-threshold beds for Set 3. For immobile beds, Q2 and Q4 events at the nearest point of the bed contribute approximately

Downloaded 13 Sep 2011 to 203.110.246.23. Redistribution subject to ASCE license or copyright. Visit http://www.ascelibrary.org

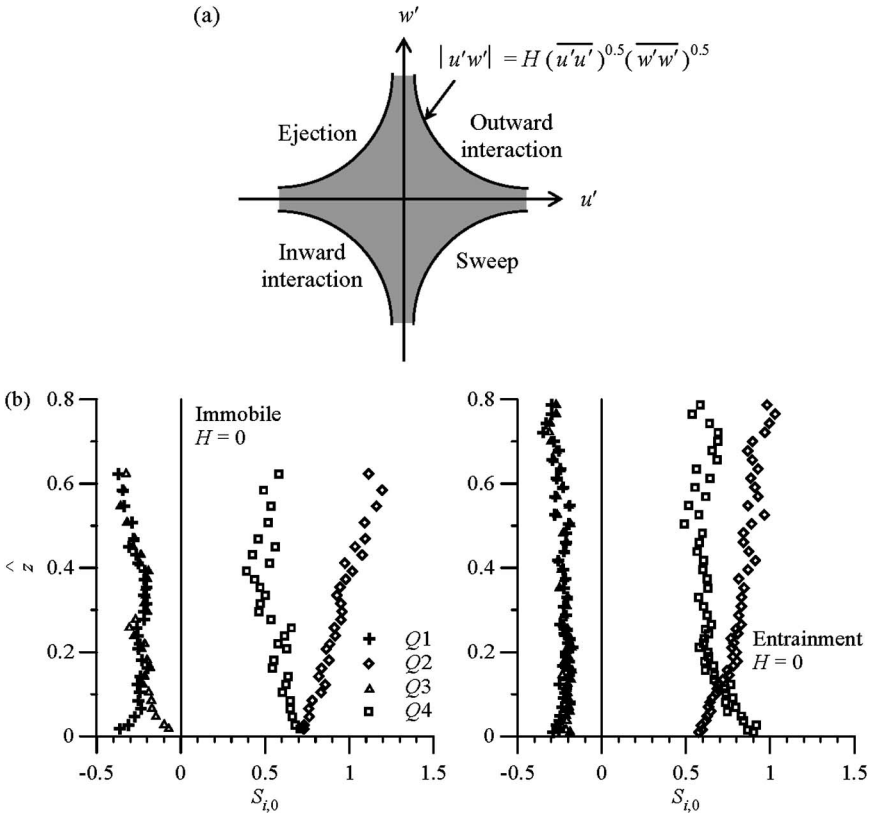

Fig. 4. (a) Quadrant analysis; (b) distributions of $S_{i,0}(\hat{z})$ for Set 3

72% to the total Reynolds shear stress production. On the other hand, near the bed, Q1 events contribute moderately by 36%; whereas Q3 events contribute minimally by 8%. To be explicit, the arrival of low-speed fluid streaks from the near-bed zone is revoked by the arrival of high-speed fluid streaks from the upper region. Thus, only a faster-moving process is prevalent in the form of outward interactions Q1. In contrast, for entrainment-threshold beds, Q4 events are the main mechanism to entrain sediments, contributing as high as approximately 90% toward the Reynolds shear stress production; whereas Q2 events contribute relatively less. The tendency of Q4 events to dominate momentum transfer over a sediment bed therefore strongly depends on the motion of surface particles. This means that sediment motion is governed by the arrival of high-speed fluid streaks. However, the contributions from Q1 and Q3 events are rather weak.

Figs. 5(a)–5(c) represent the variations of the fractional contributions $|S_{i,H}|$ of the Reynolds shear stress with hole size H for each of the four quadrants on the $u'w'$-plane at different $\hat{z}$ in flows over immobile and entrainment-threshold beds for Set 3. Contributions from all events decrease with an increase in hole size H. Nevertheless, when H becomes large, there still remain only two events, Q2 and Q4, to contribute substantially. It is obvious from Fig. 4 that the influence of an entrainment threshold of sediments on the turbulence characteristics is mainly confined to the wall-shear layer. Thus, a detailed quadrant analysis has been carried out varying the hole size H within the wall-shear layer, considering three elevations at $z = 3$ mm (nearest point to the bed), $\hat{z} = 0.12$ (within the wall-shear layer), and $\hat{z} = 0.2$ (at the top of the wall-shear layer). In Fig. 5(a) (for immobile beds), Q2 and Q4 events close to the bed give maximum contribution ($|S_{2,0}| \approx |S_{4,0}| \approx 0.72$), becoming insignificant for $H > 8$. On the other hand, Q1 events contribute moderately ($|S_{1,0}| \approx 0.38$), becoming insignificant for $H > 4$; whereas Q3 events contribute minimally ($|S_{3,0}| \approx 0.08$), vanishing for $H > 2$. Alternatively, in Fig. 5(a) (for entrainment-threshold beds), Q4 events are the governing mechanism to keep sediments in motion, giving maximum contribution ($|S_{4,0}| \approx 0.9$), whereas Q2 events contribute relatively less ($|S_{2,0}| \approx 0.6$). Both Q2 and Q4 events last over a considerable range of H, becoming insignificant for $H > 7$. However, the contributions from Q1 and Q3 events are feeble ($|S_{1,0}| \approx 0.3$ and $|S_{3,0}| \approx 0.2$) and vanish at $H = 5$ and 3, respectively. Within the wall-shear layer for immobile beds ($\hat{z} = 0.12$) [see Fig. 5(b)], Q2 events are the dominant mechanism and contribute approximately 84% ($|S_{2,0}| \approx 0.84$). On the other hand, Q4 events are relatively weak ($|S_{4,0}| \approx 0.64$), and Q1 and Q3 events are the weakest ($|S_{1,0}| \approx |S_{3,0}| \approx 0.26$). However, Q1, Q2, Q3, and Q4 events vanish at $H = 4$, 6, 3, and 5, respectively. For entrainment-threshold beds, Fig. 5(b) provides an interesting feature, where the opposing events are approximately balanced. However, Q1 and Q3 events become insignificant at $H = 4$, and Q2 and Q4 events vanish at $H = 7$. At the top of the wall-shear layer ($\hat{z} = 0.2$), Fig. 5(c) shows that the turbulent events in flows over immobile and entrainment-threshold beds have almost similar characteristics. It suggests that the influence of sediment entrainment on the turbulent flow characteristics gradually diminishes with an increase in depth and disappears at the top of the wall-shear layer. At this point ($\hat{z} = 0.2$), Q2 events are dominant ($|S_{2,0}| \approx 0.8$) with a retardation effect to the flow caused by the arrival of low-speed fluid streaks, whereas Q4 events contribute moderately $|S_{4,0}| \approx 0.6$. Both events are weakened significantly for $H > 5$. However, Q1 and Q3 events are rather weak ($|S_{1,0}| \approx |S_{3,0}| \approx 0.2$), vanishing at $H = 3$.

To study the durations and frequencies of ejection and sweep events, the occurrences of ejections or sweeps in a recorded sample were counted by fixing a hole size H and by counting the number of changeovers to the appropriate quadrant of the series of (u', w'). Then, a mean duration of ejections t_E or sweeps t_S and a mean

Downloaded 13 Sep 2011 to 203.110.246.23. Redistribution subject to ASCE license or copyright. Visit http://www.ascelibrary.org

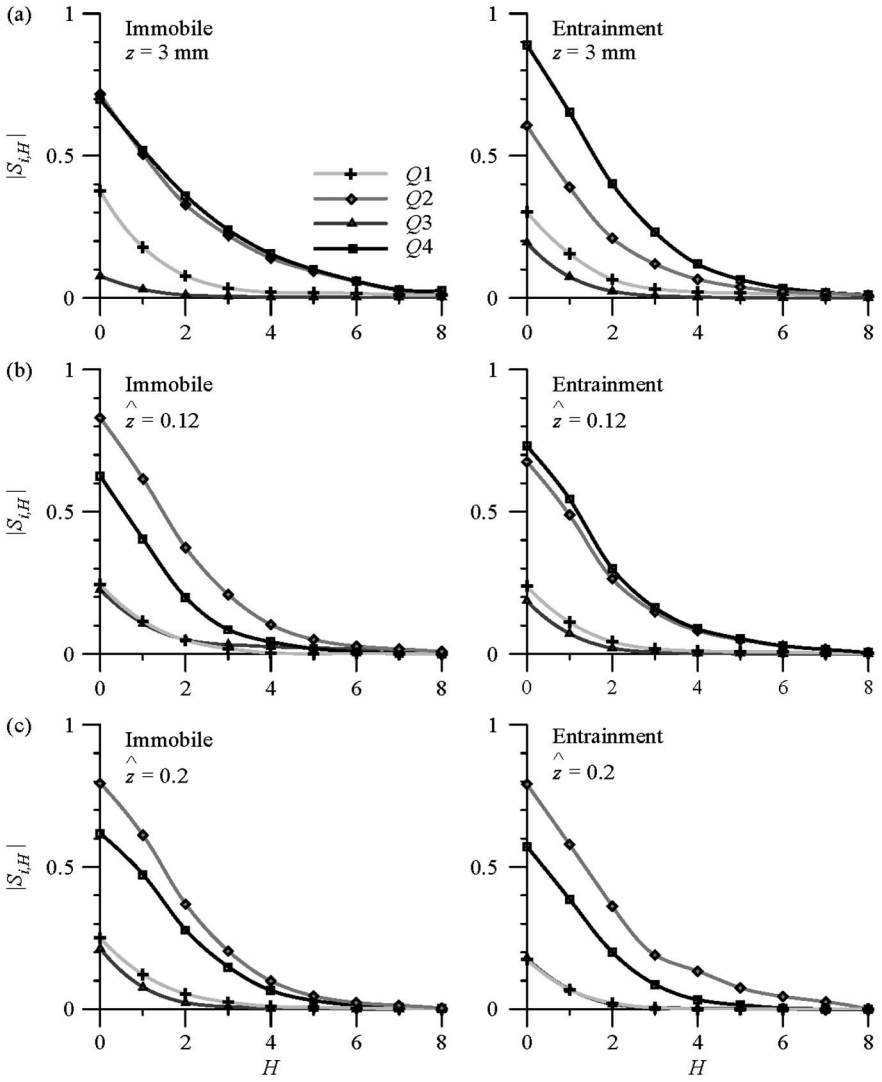

Fig. 5. Variations of $|S_{i,H}|$ with H at (a) $z = 3$ mm, (b) $\hat{z} = 0.12$ and (c) $\hat{z} = 0.2$ for Set 3

interval between ejections i_E or sweeps i_S were determined. The normalized mean durations of ejection and sweep events are represented by $T_E = t_E u_*/h$ and $T_S = t_S u_*/h$, respectively, and the normalized mean frequencies of ejection and sweep events are by $\hat{f}_E = i_E^{-1} h/u_*$ and $\hat{f}_S = i_S^{-1} h/u_*$, respectively. Figs. 6(a) and 6(b) illustrate the variations of T_E and T_S and $\hat{f}_E$ and $\hat{f}_S$ with H at $z = 3$ mm and $\hat{z} = 0.12$ and 0.2 in flows over immobile and entrainment-threshold beds for Set 3. In general, the variations of T_E and T_S are almost identical for individual bed conditions as are the variations of $\hat{f}_E$ and $\hat{f}_S$. Thus, T_E and T_S are together called *bursting duration*, and $\hat{f}_E$ and $\hat{f}_s$ are called *bursting frequency*. In Fig. 6(a), the peaks of the bursting durations occur between $1 < H < 2$, and then the durations decrease gradually with an increase in H, becoming almost invariant of H for $H > 6$. This suggests that the maximum bursting duration corresponds to the data pairs (u', w') that do not correspond to the weakest ones. The bursting duration for immobile beds is more persistent than that for entrainment-threshold beds. On the other hand, the duration is shortest close to the bed at $z = 3$ mm. Fig. 6(b) shows that the bursting frequencies decrease monotonically with an increase in H. This means that the stronger events correspond to smaller frequency. Importantly, for small values of H, the bursting for entrainment-threshold beds is more frequent than that for immobile beds. Also, the frequency increases toward the bed. Thus, it can be concluded that the mean duration of Q4 events, which govern the sediment entrainment, with relatively high frequency of occurrence, is shorter (that is, less persistent) than the mean duration of Q4 events with relatively low frequency of occurrence for immobile beds.

Flux and Advection of Reynolds Normal Stresses

Third-order correlations are directly correlated to the turbulent coherent structures because of the preservation of their signs, transmitting essential stochastic information on the temporal characteristics of the velocity fluctuations in the form of flux and advection of the turbulent stresses (Gad-el-Hak and Bandyopadhyay 1994). According to Raupach (1981), the set of third-order correlations M_{jk} are expressed as $M_{jk} = \overline{\hat{u}^j \hat{w}^k}$ with $j + k = 3$, where $\hat{u} = u'/(\overline{u'u'})^{0.5}$; and $\hat{w} = w'/(\overline{w'w'})^{0.5}$. The correlations are $M_{30} = \overline{\hat{u}^3}$, defining the streamwise flux of the streamwise Reynolds normal stress $\overline{u'u'}$, $M_{21} = \overline{\hat{u}^2 \hat{w}}$, signifying the advection of $\overline{u'u'}$ in the z-direction, $M_{12} = \overline{\hat{u}\,\hat{w}^2}$, characterizing the advection of vertical Reynolds normal stress $\overline{w'w'}$ in the x-direction, and $M_{03} = \overline{\hat{w}^3}$, providing the vertical flux of $\overline{w'w'}$.

Downloaded 13 Sep 2011 to 203.110.246.23. Redistribution subject to ASCE license or copyright. Visit http://www.ascelibrary.org

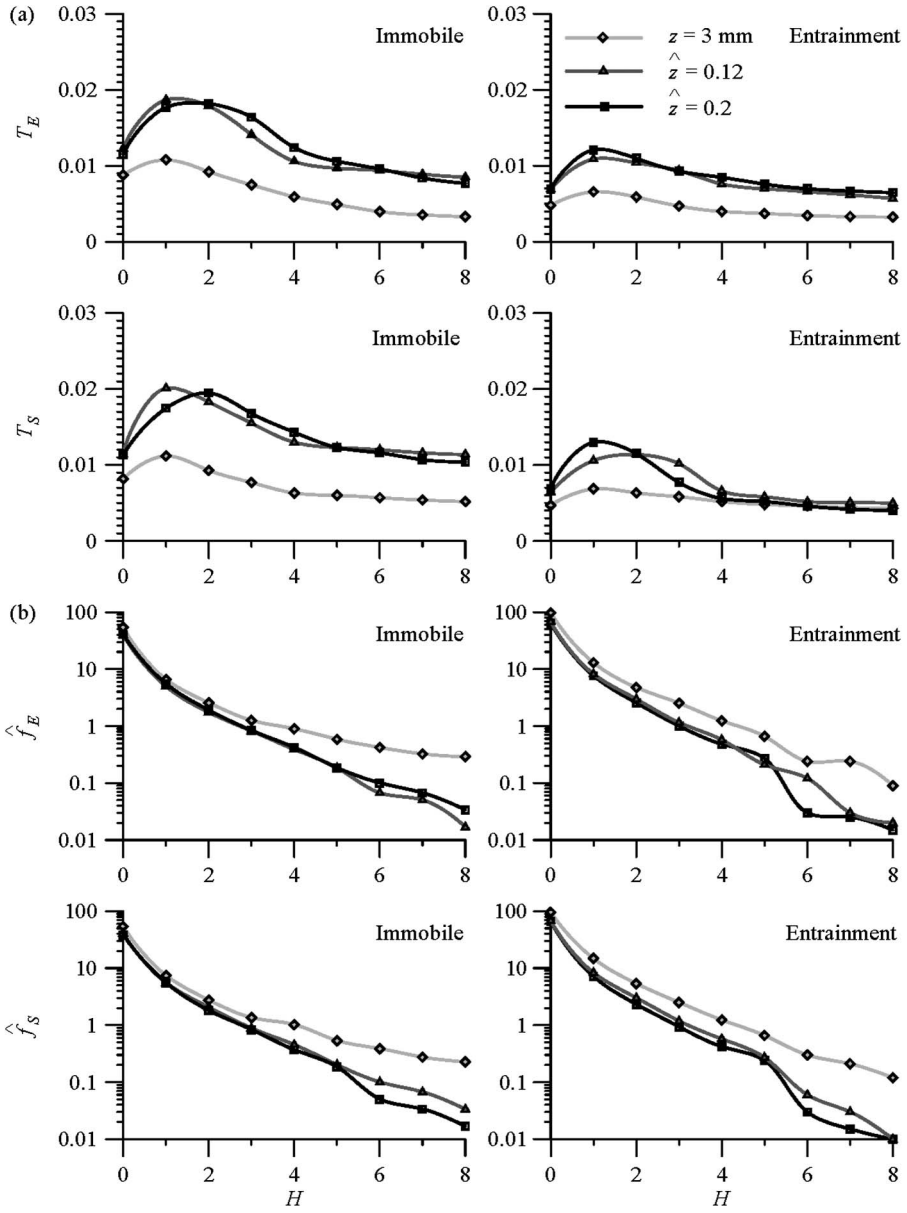

Fig. 6. (a) Mean durations of Q2 and Q4 events (T_E and T_S) as a function of H; (b) mean frequencies of Q2 and Q4 events ($\hat{f}_E$ and $\hat{f}_S$) as a function of H; data for Set 3 are presented

Figs. 7(a) and 7(b) display the vertical distributions of individual M_{jk}, where the changes are apparent within the wall-shear layer. In flows over immobile and entrainment-threshold beds [Fig. 7(a)], M_{30} starts with a positive value near the bed, changing over to a negative value for $\hat{z} > 0.14$. Near the bed, M_{30} for entrainment-threshold beds is greater than that for immobile beds, suggesting that the sediment motion influences M_{30} by increasing its magnitude, that is, by increasing the streamwise flux of $\overline{u'u'}$. On the other hand, the reverse incident takes place in the outer layer ($\hat{z} > 0.2$), where the flux of $\overline{u'u'}$ travels against the streamwise direction and is pronounced in flows over immobile beds. The mean trends of $M_{03}(\hat{z})$ and $M_{21}(\hat{z})$ for flows over immobile beds are positive over the entire flow depth, whereas those for flows over entrainment-threshold beds are negative near the bed ($\hat{z} < 0.08$) and positive for $\hat{z} > 0.08$. This means that the flux of $\overline{w'w'}$ and the advection of $\overline{u'u'}$ are in a downward direction in the near-bed flow zone over entrainment-threshold beds. In contrast, across the entire flow depth for immobile beds, the flux of $\overline{w'w'}$ and the advection of $\overline{u'u'}$ are in an upward direction. In Fig. 7(b), M_{12} starts with a small positive value near the bed, changing over to a negative value for $\hat{z} > 0.1$. Near the bed, M_{12} for entrainment-threshold beds is slightly greater than that for immobile beds, indicating that the sediment-entrainment influences M_{12} by increasing its magnitude, that is, by increasing the streamwise advection of $\overline{w'w'}$. Although the reverse event occurs in the flows for $\hat{z} > 0.1$, the advection of $\overline{w'w'}$ is prevalent against the streamwise direction for both bed conditions. The essential responses of the bursting events are plausibly recognized from these third-order correlations (Nakagawa and Nezu 1977). Near the bed, the positive M_{30} and the negative M_{03} imply strong Q4 events in flows over entrainment-threshold beds. In contrast, in flows over immobile beds, both M_{30} and M_{03} are positive, suggesting the occurrence of outward interactions Q1, as Q2 and Q4 events cancel each other, as discussed in the preceding section. In addition, the near-bed values of M_{21} and M_{12} reveal that sediment entrainment corresponds to the advection of $\overline{u'u'}$ in the downward direction and that of $\overline{w'w'}$ in the streamwise

Downloaded 13 Sep 2011 to 203.110.246.23. Redistribution subject to ASCE license or copyright. Visit http://www.ascelibrary.org

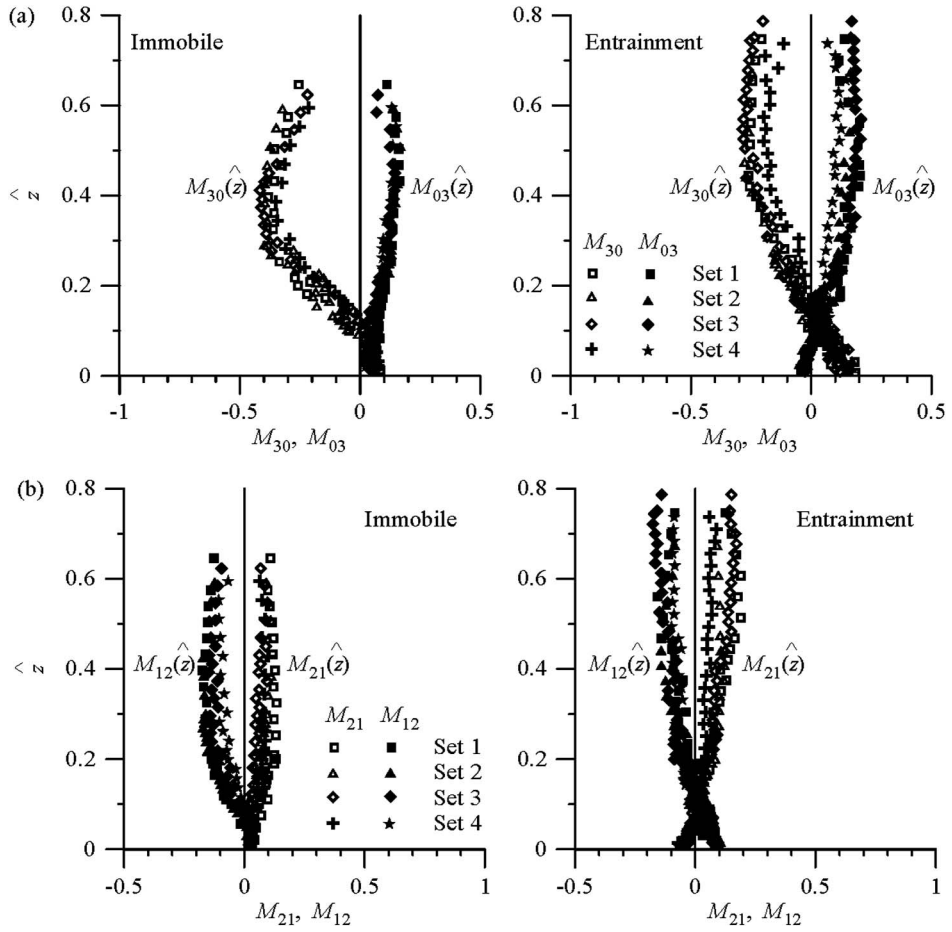

Fig. 7. Distributions of (a) flux of Reynolds normal stresses, M_{30} and M_{03}; (b) advection of Reynolds normal stresses, M_{21} and M_{12}

direction. Therefore, the analysis of third-order correlations conveys a clear message that during a sediment-entrainment regime, a streamwise acceleration is prevalent and associated with a downward flux, giving rise to Q4 events.

Turbulent Kinetic Energy and Budget

The vertical distributions of streamwise and vertical flux of the normalized turbulent kinetic energy (TKE) $F_{ku} = f_{ku}/u_*^3$ and $F_{kw} = f_{kw}/u_*^3$ in flows over immobile and entrainment-threshold beds are displayed in Fig. 8(a). In two-dimensional flows, the streamwise and vertical flux of the TKE are expressed as $f_{ku} = 0.75(\overline{u'u'u'} + \overline{u'w'w'})$ and $f_{kw} = 0.75(\overline{w'w'w'} + \overline{w'u'u'})$, respectively (Krogstad and Antonia 1999; Bey et al. 2007). In Fig. 8(a), the streamwise flux of the TKE F_{ku} starts with a positive value near the bed, which becomes negative for $\hat{z} > 0.15$, suggesting that the TKE flux transports in the streamwise direction within the wall-shear layer. On the other hand, F_{ku} is negative in the outer layer, suggesting a transport of TKE flux against the streamwise direction. Essentially, the inertia of fluid streaks in this zone induces a retarding effect, resulting in a negative F_{ku}. It is evident that in the near-bed zone, the peak positive value of F_{ku} in flows over entrainment-threshold beds is greater than that of F_{ku} in flows over immobile beds. In contrast, the positive value of vertical flux F_{kw} over the entire flow depth for immobile beds indicates an upward transport of TKE flux, whereas in the near-bed flow zone ($\hat{z} < 0.1$), a negative value of F_{kw} in flows over entrainment-threshold beds implies the downward transport of TKE flux. Therefore, the most important feature of a sediment-entrainment regime lies on the near-bed flow zone, where the positive value of F_{ku} and the negative value of F_{kw} compose the Q4 events. On the other hand, for immobile beds, both the positive values of F_{ku} and F_{kw} form the Q1 events. Therefore, it is concluded that the influence of sediment entrainment is noticeable in the distributions of F_{ku} and F_{kw}.

The TKE budget in two-dimensional flows is constituted by the turbulent production $t_P = -\overline{u'w'}(\partial u/\partial z)$, which is balanced by the summation of the turbulent dissipation ε, turbulent energy diffusion $t_D = \partial f_{kw}/\partial z$, pressure energy diffusion $p_D = \partial(\overline{p'w'/\rho})/\partial z$, and viscous diffusion $v_D = -\upsilon(\partial^2 k/\partial z^2)$, where p' = pressure fluctuations; and k = TKE (Nezu and Nakagawa 1993). The viscous diffusion v_D is insignificant when the turbulent-rough flows have the shear-particle Reynolds numbers R_* greater than 70. To evaluate ε, the relationship $\varepsilon = (15\upsilon/u^2)\overline{(\partial u'/\partial t)^2}$ is used, as was done by Irwin (1973) and Krogstad and Antonia (1999). The pressure energy diffusion p_D is thus estimated from the TKE budget relationship as $p_D = t_P - \varepsilon - t_D$. Fig. 8(b) illustrates the TKE budget in flows over immobile and entrainment-threshold beds for Set 3. The parameters of the TKE budget are expressed in normalized form as T_P, E_D, T_D, and $P_D = (t_P, \varepsilon, t_D, p_D) \times (h/u_*^3)$. In general, turbulent production T_P increases near the bed with an increase in $\hat{z}$ of up to $\hat{z} > 0.05$ and then decreases rapidly, becoming nearly constant (with a small magnitude) for $\hat{z} > 0.3$. The trend of E_D that has a near-bed amplification decreases monotonically with an increase in $\hat{z}$. A positive value of T_P corresponds to the conversion of energy from the time-averaged flow to the turbulence. The distributions of E_D have a distinct lag from those of T_P. The influence of sediment

Downloaded 13 Sep 2011 to 203.110.246.23. Redistribution subject to ASCE license or copyright. Visit http://www.ascelibrary.org

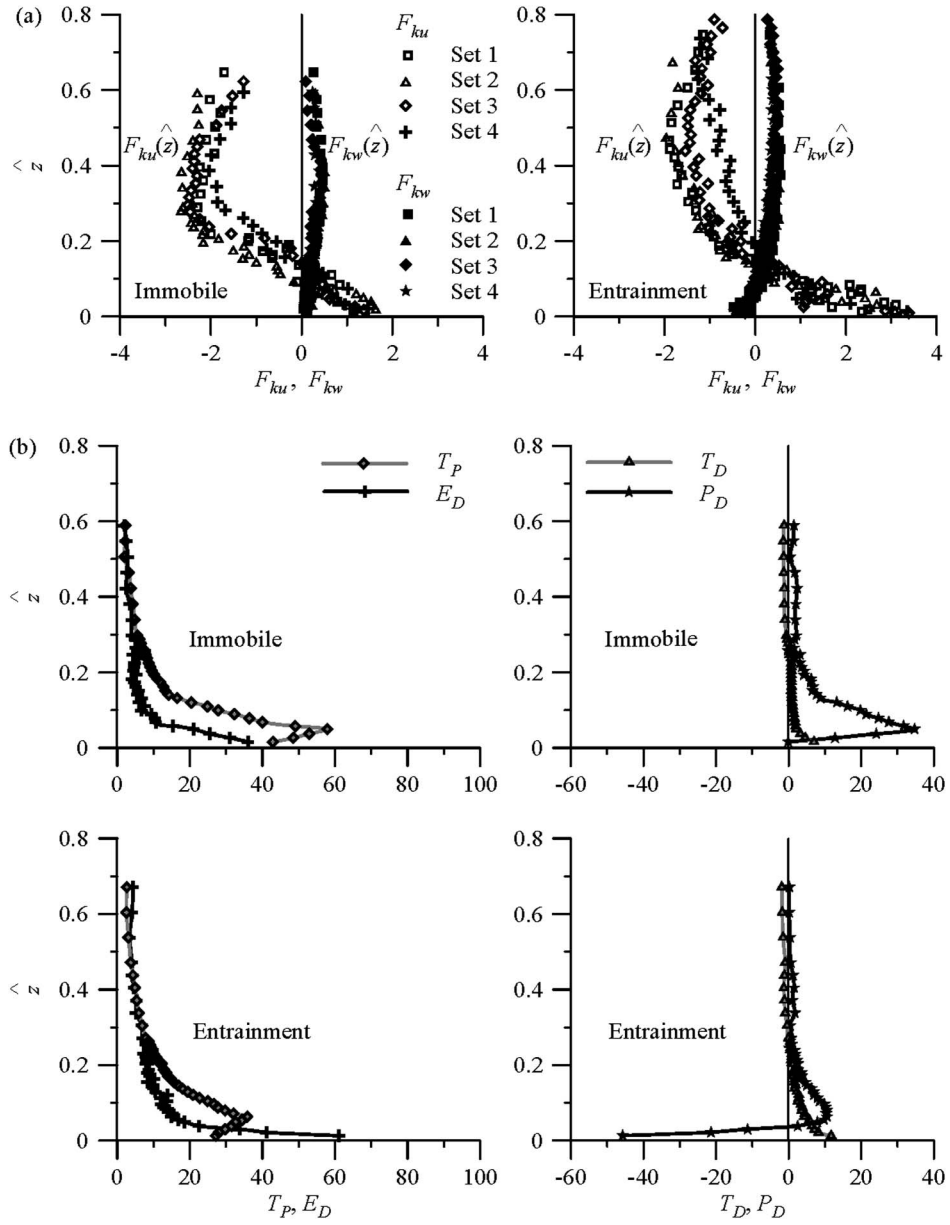

Fig. 8. (a) Distributions of streamwise and vertical flux of TKE, F_{ku} and F_{kw}; (b) TKE budget for Set 3

entrainment is apparent in the near-bed distributions of T_P and E_D, where the lag is reversed, i.e., $E_D > T_P$. To be explicit, the effect of sediment entrainment is to reduce T_P and increase E_D. The near-bed reduction of T_P has an impact on $\tilde{u}$ distributions [see Fig. 3(a)] with sediment entrainment because the conversion of less energy from the time-averaged flow to the turbulence causes less departure in $\tilde{u}$ distributions from the logarithmic law. Essentially, the difference of T_P and E_D at any depth $\hat{z}$ is balanced by the combination of T_D and P_D. The T_D decreases monotonically with an increase in $\hat{z}$ within the wall-shear layer and then becomes almost invariant of $\hat{z}$ with a small magnitude. On the other hand, P_D attains a positive peak at $\hat{z} \approx 0.05$ and then gradually decreases with an increase in $\hat{z}$, becoming a constant with a small magnitude. The most interesting feature lies on the near-bed distributions of P_D in flows over entrainment-threshold beds. It is apparent that sediment entrainment is associated with a drastic changeover of P_D to a large negative value ($P_D = -45$). The negative value of P_D indicates a gain in turbulent production. Therefore, in near-bed flow over entrainment-threshold beds, the turbulent dissipation exceeds the turbulent production, and the pressure energy diffusion is considerably negative. These findings are in agreement with Detert et al. (2010), showing that the entrainment of bed particles is likely to be associated with a low-pressure flow pattern.

Conclusions

Experiments were conducted to quantify the turbulence characteristics of near-bed flows at an entrainment threshold of noncohesive sediments. Analysis of experimental data measured by a Vectrino probe in flows over both immobile and entrainment-threshold sediment beds reveals the changes in the turbulent characteristics caused by difference in bed conditions. The influence of an entrainment threshold of sediments on the turbulence characteristics is mainly confined to the wall-shear layer that characterizes the near-bed flow zone. However, the turbulence characteristics in the outer layer of flows are generally indistinguishable for immobile or entrainment-threshold beds. In the near-bed flow zone, there

Downloaded 13 Sep 2011 to 203.110.246.23. Redistribution subject to ASCE license or copyright. Visit http://www.ascelibrary.org

exists a departure in the distributions of the observed time-averaged streamwise velocity from the logarithmic law because of the roughness layer created by the sediment particles. The departure of the velocity data plots for immobile beds from the logarithmic law is greater than that for entrainment-threshold beds. The near-bed distributions of the Reynolds shear stress for immobile and entrainment-threshold beds also deviate from the linear law of the Reynolds shear stress, having a relatively high damping in the distributions with entrainment-threshold beds. The damping of the Reynolds shear stress is attributed to the provided momentum for the flow to maintain bed-particle motion. The quadrant analysis of the data of velocity fluctuations corroborates that ejection and sweep events in the near-bed flow zone for immobile beds rescind each other, giving rise to the outward interactions, whereas sweep events are the prevailing mechanism toward sediment entrainment. On the other hand, ejection events are prevalent at the top of the wall-shear layer. The bursting duration for entrainment-threshold beds is shorter than that for immobile beds, whereas the bursting frequency for entrainment-threshold beds is larger than that for immobile beds. The third-order correlations imply that a streamwise acceleration is prevalent during sediment entrainment and associated with a downward flux, suggesting sweep events with a downward advection of the streamwise Reynolds normal stress. An entrainment threshold of sediments is associated with an increased near-bed positive value of streamwise flux of TKE that migrates in the streamwise direction and a negative value of vertical flux of TKE that migrates downward. The TKE budget indicates that for entrainment-threshold beds, the turbulent dissipation is greater than the turbulent production, and the pressure energy diffusion becomes drastically negative, which implies a gain in turbulent production. These findings can be used in the formulation of new models relating to the near-bed turbulence, particularly, turbulence bursting, and to the entrainment of sediment particles via physically based schematizations.

As a future scope of research, the findings of the study raise a number of theoretical issues that can address how to analyze sediment entrainment, the most important of which is how best to include the sweep events into a theoretical model of the sediment-entrainment process and how the sweep events, including their duration and frequency, contribute toward the near-bed Reynolds shear stress production. In near-bed flow zone, a gain in turbulent production attributable to negative pressure energy diffusion is another important aspect that can be considered in a theoretical model. A new paramerization of the Basset term that contains temporal change of velocity (acceleration) of fluid with respect to that of a particle could also be found for a numerical model of sediment entrainment. The possible implications of the changes of a turbulent flow boundary layer structure caused by sediment motion could be as follows.

Parker et al. (2003) proposed an entrainment formulation according to which the average concentration of particles in motion can be expressed as an increasing function of the excess of the residual shear stress (defined as the difference between the fluid residual shear stress on the bed and its critical value). The rationale behind this formulation is that the residual shear stress can be taken as a measure of the residual turbulent events close to the bed; hence, it represents the ability of the flow to produce those turbulent events, which appear to be the major hydrodynamic cause for the entrainment. In this context, because of the lack of detailed experimental observations, Parker et al. (2003) assumed a linear relationship between the average concentration of moving particles and the excess of the residual shear stress. Therefore, the present experimental findings show the relation between the residual fluid shear stress at the bed and the turbulent events in the shear boundary layer. Moreover, the results of this study can be used to calculate the overall transfer of momentum from the fluid to the solid phase and the residual fluid shear stress on the bed. These results therefore allow researchers (1) to elaborate a more accurate parameterization for the reduction of Reynolds shear stress in the presence of entrainment; and (2) to define a relation between the average concentration of particles in motion and the residual shear stress.

Notation

The following symbols are used in this paper:

d_{50} = median diameter of sediment (L);
E_D = normalized turbulent dissipation;
F = flow Froude number;
F_d = densimetric Froude number;
F_{ku} = normalized streamwise flux of turbulent kinetic energy, $f_{ku}/u*^3$;
F_{kw} = normalized vertical flux of turbulent kinetic energy, f_{kw}/u_*^3;
f = frequency (T^{-1});
$\hat{f}_E$ = normalized mean frequency of ejections;
f_{ku} = streamwise flux of turbulent kinetic energy, $0.75(\overline{u'u'u'} + \overline{u'w'w'})$ (L^3T^{-3});
f_{kw} = vertical flux of turbulent kinetic energy, $0.75(\overline{w'w'w'} + \overline{w'u'u'})$ (L^3T^{-3});
$\hat{f}_S$ = normalized mean frequency of sweeps;
g = gravitational acceleration (LT^{-2});
H = hole-size parameter;
h = flow depth (L);
i = quadrant number;
i_E = mean interval between ejections (T);
i_S = mean interval between sweeps (T);
k = turbulent kinetic energy (L^2T^{-2});
M_{jk} = third-order correlations;
n = number of bed particles per unit area;
P_D = normalized pressure energy diffusion;
p_D = pressure energy diffusion (L^2T^{-3});
p' = pressure fluctuations ($ML^{-1}T^{-2}$);
q_s = sediment transport rate ($ML^{-1}T^{-1}$);
R = flow Reynolds number;
R_* = shear-particle Reynolds number;
S = streamwise bed slope;
$S_{i,H}$ = fractional contribution toward Reynolds shear stress production from bursting events;
S_{ii} = velocity power spectra (L^2T^{-1});
S_h = relative submergence;
s = relative density of sediment;
T = sampling time (T);
T_D = normalized turbulent energy diffusion;
T_E = normalized mean duration of ejections;
T_P = normalized turbulent production;
T_S = normalized mean duration of sweeps;
t = time (T);
t_D = turbulent energy diffusion (L^2T^{-3});
t_E = mean duration of ejections (T);
t_P = turbulent production (L^2T^{-3});
t_S = mean duration of sweeps (T);
U = depth-averaged flow velocity (LT^{-1});
u = time-averaged streamwise velocity component (LT^{-1});
$\tilde{u}$ = normalized time-averaged streamwise velocity;
$\hat{u} = u'/(\overline{u'u'})^{0.5}$;
u' = fluctuations of streamwise velocity (LT^{-1});

Downloaded 13 Sep 2011 to 203.110.246.23. Redistribution subject to ASCE license or copyright. Visit http://www.ascelibrary.org

u_* = shear velocity (LT^{-1});
u_{*1} = shear velocity obtained from bed slope (LT^{-1});
u_{*2} = shear velocity obtained from Reynolds shear stress (LT^{-1});
uw^+ = normalized Reynolds shear stress;
v = time-averaged lateral velocity component (LT^{-1});
v' = fluctuations of lateral velocity (LT^{-1});
v_D = viscous diffusion (L^2T^{-3});
w = time-averaged vertical velocity component (LT^{-1});
$\hat{w}$ = $w'/(\overline{w'w'})^{0.5}$;
w' = fluctuations of vertical velocity (LT^{-1});
x = streamwise distance (L);
z = vertical distance (L);
$\hat{z}$ = z/h;
z^+ = z/d_{50};
Δ = submerged relative density of sediment;
ε = turbulent dissipation (L^2T^{-3});
Θ = Shields parameter;
λ = friction factor;
$\lambda_{i,H}$ = detection function;
μ = Coulomb friction factor;
ξ = fraction of particles entrained per unit area;
ρ = mass density of fluid (ML^{-3});
ρ_0 = porosity of sediments;
σ_g = geometric standard deviation;
τ = total bed shear stress ($ML^{-1}T^{-2}$);
τ_f = bed shear stress of fluid ($ML^{-1}T^{-2}$);
τ_s = shear stress to overcome frictional resistance ($ML^{-1}T^{-2}$) and;
υ = kinematic viscosity of fluid (L^2T^{-1}).

References

Best, J. (1992). "On the entrainment of sediment and initiation of bed defects: Insights from recent developments within turbulent boundary layer research." *Sedimentology*, 39(5), 797–811.

Bey, A., Faruque, M. A. A., and Balachandar, R. (2007). "Two-dimensional scour hole problem: Role of fluid structures." *J. Hydraul. Eng.*, 133(4), 414–430.

Cao, Z. (1997). "Turbulent bursting-based sediment entrainment function." *J. Hydraul. Eng.*, 123(3), 233–236.

Clifford, N. J., McClatchey, J., and French, J. R. (1991). "Measurements of turbulence in the benthic boundary layer over a gravel bed and comparison between acoustic measurements and predictions of the bedload transport of marine gravels." *Sedimentology*, 38(1), 161–171.

Detert, M., Weitbrecht, V., and Jinka, G. H. (2010). "Laboratory measurements on turbulent pressure fluctuations in and above gravel beds." *J. Hydraul. Eng.*, 136(10), 779–789.

Dey, S. (1999). "Sediment threshold." *Appl. Math. Modell.*, 23(5), 399–417.

Dey, S., Bose, S. K., and Sastry, G. L. N. (1995). "Clear water scour at circular piers: A model." *J. Hydraul. Eng.*, 121(12), 869–876.

Dey, S., Dey Sarker, H. K., and Debnath, K. (1999). "Sediment threshold under stream flow on horizontal and sloping beds." *J. Eng. Mech.*, 125(5), 545–553.

Dey, S., and Papanicolaou, A. (2008). "Sediment threshold under stream flow: A state-of-the-art review." *J. Civil Eng.*, 12(1), 45–60.

Dey, S., and Raikar, R. V. (2007). "Characteristics of loose rough boundary streams at near-threshold." *J. Hydraul. Eng.*, 133(3), 288–304.

Drake, T. G., Shreve, R. L., Dietrich, W. E., Whiting, P. J., and Leopold, L. B. (1988). "Bedload transport of fine gravel observed by motion picture photography." *J. Fluid Mech.*, 192, 193–217.

Dwivedi, A., Melville, B. W., Shamseldin, A. Y., and Guha, T. K. (2010a). "Drag force on a sediment particle from point velocity measurements: A spectral approach." *Water Resour. Res.*, 46, W10529.

Dwivedi, A., Melville, B., and Shamseldin, A. Y. (2010b). "Hydrodynamic forces generated on a spherical sediment particle during entrainment." *J. Hydraul. Eng.*, 136(10), 756–769.

Fenton, J. D., and Abbott, J. E. (1977). "Initial movement of grains on a stream bed: The effect of relative protrusion." *Proc. R. Soc. London, Ser. A*, 352(1671), 523–537.

Gad-el-Hak, M., and Bandyopadhyay, P. R. (1994). "Reynolds number effects in wall-bound turbulent flow." *Appl. Mech. Rev.*, 47(8), 307–365.

Gaudio, R., Miglio, A., and Dey, S. (2010). "Non-universality of von Kármán's κ in fluvial streams." *J. Hydraul. Res.*, 48(5), 658–663.

Grass, A. J. (1970). "Initial instability of fine bed sand." *J. Hydraul. Div.*, 96(3), 619–632.

Heathershaw, A. D., and Thorne, P. D. (1985). "Sea-bed noises reveal role of turbulent bursting phenomenon in sediment transport by tidal currents." *Nature*, 316(6026), 339–342.

Hofland, B., and Battjes, J. A. (2006). "Probability density function of instantaneous drag forces and shear stresses on a bed." *J. Hydraul. Eng.*, 132(11), 1169–1175.

Irwin, H. P. A. H. (1973). "Measurements in a self-preserving plane wall jet in a positive pressure gradient." *J. Fluid Mech.*, 61, 33–63.

Kline, S. J., Reynolds, W. C., Schraub, F. A., and Runstadler, P. W. (1967). "The structure of turbulent boundary layers." *J. Fluid Mech.*, 30, 741–773.

Krogstad, P. Å., and Antonia, R. A. (1999). "Surface roughness effects in turbulent boundary layers." *Exp. Fluids*, 27(5), 450–460.

Krogstad, P. A., Antonia, R. A., and Browne, L. W. B. (1992). "Comparison between rough and smooth wall turbulent boundary layers." *J. Fluid Mech.*, 245, 599–617.

Lu, H., Raupach, M. R., and Richards, K. S. (2005). "Modeling entrainment of sedimentary particles by wind and water: A generalized approach." *J. Geophys. Res.*, 110, D24114.

Lu, S. S., and Willmarth, W. W. (1973). "Measurements of the structures of the Reynolds stress in a turbulent boundary layer." *J. Fluid Mech.*, 60, 481–511.

Nakagawa, H., and Nezu, I. (1977). "Prediction of the contributions to the Reynolds stress from bursting events in open-channel flows." *J. Fluid Mech.*, 80, 99–128.

Nelson, J. M., Shreve, R. L., McLean, S. R., and Drake, T. G. (1995). "Role of near-bed turbulence structure in bed load transport and bed form mechanics." *Water Resour. Res.*, 31(8), 2071–2086.

Nezu, I., and Nakagawa, H. (1993). *Turbulence in open-channel flows*, Balkema, Rotterdam, Netherlands.

Nikora, V. (1999). "Origin of the "−1" spectral law in wall-bound turbulence." *Phys. Rev. Lett.*, 83(4), 734–736.

Nikora, V., and Goring, D. (2000). "Flow turbulence over fixed and weakly mobile gravel beds." *J. Hydraul. Eng.*, 126(9), 679–690.

Nikora, V., Goring, D., McEwan, I., and Griffiths, G. (2001). "Spatially averaged open-channel flow over rough bed." *J. Hydraul. Eng.*, 127(2), 123–133.

Papanicolaou, A. N., Diplas, P., Dancey, C., and Balakrishnan, M. (2001). "Surface roughness effects in near-bed turbulence: Implications to sediment entrainment." *J. Eng. Mech.*, 127(3), 211–218.

Parker, G., Seminara, G., and Solari, L. (2003). "Bedload at low shields stress on arbitrarily sloping beds: Alternative entrainment formulation." *Water Resour. Res.*, 39, 1249.

Raupach, M. R. (1981). "Conditional statistics of Reynolds stress in rough-wall and smooth-wall turbulent boundary layers." *J. Fluid Mech.*, 108, 363–382.

Raupach, M. R., Antonia, R. A., and Rajagopalan, S. (1991). "Rough-wall turbulent boundary layers." *Appl. Mech. Rev.*, 44(1), 1–25.

Robinson, S. K. (1991). "The kinematics of turbulent boundary layer structure." *NASA TM-103859*, Ames Research Center, Moffett Field, CA.

Schmeeckle, M. W., Nelson, J. M., and Shreve, R. L. (2007). "Forces on stationary particles in near-bed turbulent flows." *J. Geophys. Res.*, 112, F02003.

Shields, A. F. (1936). "Application of similarity principles and turbulence research to bed-load movement." *Mitteilungen der Preussischen Versuchsanstalt für Wasserbau und Schiffbau*, 26, 5–24 (in German).

Song, T., Chiew, Y. M., and Chin, C. O. (1998). "Effect of bed-load movement on flow friction factor." *J. Hydraul. Eng.*, 124(2), 165–175.

Downloaded 13 Sep 2011 to 203.110.246.23. Redistribution subject to ASCE license or copyright. Visit http://www.ascelibrary.org

Song, T., Graf, W. H., and Lemmin, U. (1994). "Uniform flow in open channels with movable gravel bed." *J. Hydraul. Res.*, 32(6), 861–876.
Streeter, V. L., and Wylie, E. B. (1983). *Fluid mechanics*, McGraw-Hill, New York.
Sutherland, A. J. (1967). "Proposed mechanism for sediment entrainment by turbulent flows." *J. Geophys. Res.*, 72, 6183–6194.
Thorne, P. D., Williams, J. J., and Heathershaw, A. D. (1989). "In situ acoustic measurements of marine gravel threshold and transport." *Sedimentology*, 36(1), 61–74.
U.S. Army Engrs. Waterways Experiment Station (USAE-WES). (1936). "Flume tests made to develop a synthetic sand which will not form ripples when used in movable bed models." *Tech. Memo. 99-1*, Viksburg, MS.
van Rijn, L. C. (1984). "Sediment transport, part I: Bed-load transport." *J. Hydraul. Eng.*, 110(10), 1431–1456.
Yang, S. Q., Tan, S. K., and Lim, S. Y. (2004). "Velocity distribution and dip-phenomenon in smooth uniform open channel flows." *J. Hydraul. Eng.*, 130(12), 1179–1186.
Yeganeh-Bakhtiary, A., Gotoh, H., and Sakai, T. (2000). "Applicability of the Euler-Lagrange coupling multiphase-flow model to bed-load transport under high bottom shear." *J. Hydraul. Res.*, 38(5), 389–398.
Yeganeh-Bakhtiary, A., Shabani, B., Gotoh, H., and Wang, S. S. Y. (2009). "A three-dimensional distinct element model for bed-load transport." *J. Hydraul. Res.*, 47(2), 203–212.
White, C. M. (1940). "The equilibrium of grains on the bed of a stream." *Proc. Royal. Soc., Ser. A*, 174(958), 322–338.
Zanke, U. C. E. (2003). "On the influence of turbulence on the initiation of sediment motion." *Int. J. Sediment Res.*, 18(1), 17–31.

Downloaded 13 Sep 2011 to 203.110.246.23. Redistribution subject to ASCE license or copyright. Visit http://www.ascelibrary.org